Research Article | Vol. 10, No. 9 / 1 September 2020 / Optical Materials Express 2254
Optical Materials EXPRESS

Ultraviolet hollow-core waveguides with sub-unitary index chalcogenide cladding

JINXIANG LI,[1] BEHRAD GHOLIPOUR,[1,2,3,5] DAVIDE PICCINOTTI,[1,2] KEVIN F. MACDONALD,[1,6] AND NIKOLAY I. ZHELUDEV[1,4]

[1]*Optoelectronics Research Centre and Centre for Photonic Metamaterials, University of Southampton, Highfield, Southampton SO17 1BJ, UK*
[2]*Department of Chemistry, University of Southampton, Highfield, Southampton SO17 1BJ, UK*
[3]*Department of Electrical and Computer Engineering, University of Alberta, Edmonton, Alberta T6G 1H9, Canada*
[4]*Centre for Disruptive Photonic Technologies & The Photonics Institute, School of Physical and Mathematical Sciences, Nanyang Technological University, Singapore 637371, Singapore*
[5]*bgholipo@ualberta.ca*
[6]*kfm@orc.soton.ac.uk*

Abstract: The chalcogenide semiconductor antimony telluride exhibits a sub-unitary refractive index as low as 0.7 at mid- to near-UV wavelengths between 220 and 400 nm, with the spectral width of the sub-unitary band, minimum index and associated extinction coefficient being controllable functions of alloy composition. As such it can enable step-index hollow-core optical waveguiding at ultraviolet wavelengths and thereby, for example, spectroscopic and sensing applications wherein the confinement of light and a fluid analyte in the same core volume maximizes sensitivity, thereby limiting required interaction lengths to as little as a few wavelengths.

1. Introduction

Waveguiding in the ultraviolet spectral range can play an important role in a wide range of applications including from atomic and molecular physics (laser cooling and coherent manipulation of trapped ions with transitions in the UV; atomic clocks) and UV Raman spectroscopy to frequency conversion (frequency comb and high-harmonic generation), and biochemical and gas sensing [1–7]. To these ends, a variety of integrated photonics platforms based on high-refractive-index media such as beta-barium borate [3], aluminum oxide [4] and aluminum nitride [1,5,6], have been investigated in the UV spectral range. At any wavelength, hollow-core waveguide architectures are of particular technological interest to spectroscopic and sensing applications because they provide for the confinement of both light and a fluid (gaseous or liquid) analyte in the same space, thereby facilitating strong light-analyte interactions over relatively short propagation lengths. Light guiding in hollow-core architectures can be based either upon a precisely microstructured (photonic crystal, Bragg or anti-resonant) cladding [8–12], or a simple step-index cross-sectional profile - the latter being generally more amenable to planar fabrication techniques, and thereby to optoelectronic device integration, e.g. with light emitters and detectors, and for lab-on-chip applications. However, the step-index geometry requires a cladding medium with an intrinsic refractive index n lower than that of the core at the operating wavelength, which is to say <1 in the case of an air or vacuum core. Here we show that certain chalcogenide semiconductors with sub-unitary refractive indices over a band of wavelengths extending from around 220 to 400 nm, depending on alloy composition, may be employed as cladding materials for UV hollow-core waveguides.

#400058 https://doi.org/10.1364/OME.400058
Journal © 2020 Received 12 Jun 2020; revised 29 Jul 2020; accepted 31 Jul 2020; published 24 Aug 2020

Optical Materials EXPRESS

Chalcogenides are compounds based upon group-16 elements (sulphur, selenium and tellurium) covalently bound to 'network formers' such as arsenic, germanium, antimony and gallium. They have found a wide range of photonic and optoelectronic applications based upon their infrared transparency, high optical nonlinearity, photo-tunability, and capacity for non-volatile structural phase switching [13–15]. They are also noted for their exceptional compositional variety – the fact that their optical, electronic and physical properties depend strongly upon (i.e. can be controlled by varying) stoichiometry [16,17]. In most applications and research contexts (at visible to mid-infrared wavelengths) they are employed as high-index, transparent dielectric and phase-change media. However, certain compositions have also been recognized recently as UV-visible plasmonic materials [17–21] and (in monocrystalline form) topological insulators [22–24]. However, little note has been taken of the fact that various chalcogenide compositions have refractive indices that are lower than the majority of oxides, nitrides, perovskites, etc., and specifically values of $n < 1$, in the near- to mid-UV (UVA to lower-energy UVC) spectral range.

2. Results and discussion

A systematic study of optical properties in the bismuth antimony telluride (Bi:Sb:Te or BST) alloy system [17], using high-throughput physical vapor deposition and characterization techniques, has shown that SbTe binaries in particular (which are otherwise known as thermoelectric [25] and phase-change [26] media) can present UV refractive indices as low as 0.7 (Fig. 1): Precisely controlled co-deposition from elemental sources produces a thin film with a known, continuous compositional gradient, providing for systematic correlation of optical (electrical, thermal, etc.) properties with composition. It is found (Fig. 1) that minimum index generally decreases with increasing Sb:Te at% ratio, while at the same time the spectral position of said minimum and the spectral width of the band over which $n < 1$ increases (extending at maximum from around 220 to 400 nm). Extinction coefficients κ also depend upon stoichiometry, being lowest at shorter wavelengths (within the range of interest here – Fig. 1(b)) and increasing with increasing Sb:Te at% ratio. We note that absolute values of the extinction coefficient here are high as compared to those of materials that would conventionally be considered for most waveguiding applications. However, when modes are strongly confined to a hollow core, intrinsic losses in the cladding medium are of reduced consequence and are thereby not prohibitive to short-reach applications that would be otherwise inaccessible at UV wavelengths.

We consider two archetypal hollow-core waveguide geometries (Fig. 2): a cylindrical step-index optical fiber configuration comprising an air/vacuum core of diameter d surrounded by an SbTe cladding of (for simplicity of modelling) infinite radial extent; and a planar geometry (that would be amenable to planar lithographic fabrication processes) wherein a square-section air/vacuum core of side length h is surrounded by SbTe. An eigenvalue solver based on the finite-difference time-domain (FDTD) technique is employed to obtain the effective refractive index n_{eff}, extinction coefficient κ_{eff}, and cross-sectional electromagnetic field distributions for the modes of such waveguides. The models employ a non-uniform mesh with a minimum grid size of 5 nm in the core and perfectly matched layer (PML) boundary conditions. With knowledge of the effective index and extinction coefficient of a mode, its complex wavevector component in the propagation direction is given by $\beta = 2\pi/(n_{eff} + i\kappa_{eff})$, and the propagation distance (over which intensity falls by a factor of 1/e) by $L^* = 1/2Im\{\beta\} = \lambda/4\pi\kappa_{eff}$, where λ is the free-space wavelength.

Figure 2 presents effective parameters for the TE_{00} and HE_{11} modes respectively of square- and circular-section (planar and fiber) waveguides – for practical purposes, the modes to which light could most readily be coupled from a free-space (Gaussian) beam or another (conventional solid core, single-mode) guide, and the TE_{01} fiber mode, which offers the lowest propagation loss overall. (Launching the latter in an unstructured fiber requires matching of the phase, amplitude, and polarization state, e.g. using 'Pancharatnam-Berry phase optical elements' [27] or combination of a spatial light modulator and waveplates [28].) Data are plotted here only for

Optical Materials EXPRESS

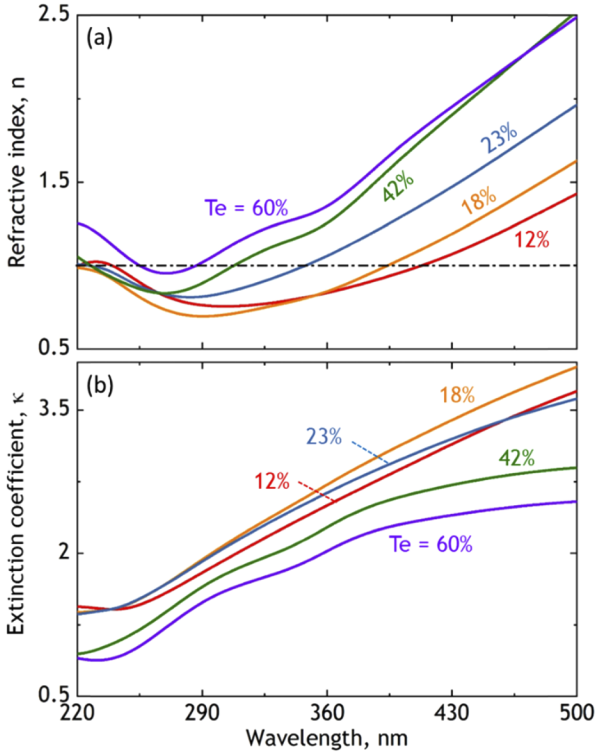

Fig. 1. Compositional tuning of SbTe optical properties. UV to high-energy visible spectral dispersion of (a) refractive index and (b) extinction coefficient for as-deposited antimony telluride for a selection of compositional ratios [labelled by Te at%], evaluated by variable angle spectroscopic ellipsometry [17].

the range of wavelengths over which each SbTe composition supports hollow-core waveguiding, i.e. over which $n < n_{eff} < 1$. In all cases, n_{eff} is a monotonic function of wavelength almost entirely independent of SbTe composition, which is to say almost insensitive to the values (Fig. 1) of the cladding refractive index (so long as it meets the condition of being <1) or extinction coefficient. This is because the effective index is simply the ratio of the speed of light in vacuum to its speed in the guided mode under consideration. The modes here are all strongly confined to the hollow (i.e. vacuum) core and therefore present a mode index uniformly close to one – small differences amongst n_{eff} values for the different modes at a given wavelength can be taken to be representative of differences in the extent of confinement. The spectral dispersion of n_{eff} is a function core size versus wavelength.

In contrast, κ_{eff} values are a function of cladding composition. For each composition, they decrease (for the most part) monotonically with wavelength as do the SbTe κ values (Fig. 1(b)). However, for a given wavelength the lowest guided mode κ_{eff} values are not found for the composition simply with the lowest value of κ, because they also depend upon the magnitude of index contrast between core and cladding (see insets to Figs. 2(d)–2(f)). As such, the 18at% Te alloy ($Sb_{4.1}Te_{0.9}$) generally yields the lowest κ_{eff} values, and therefore lowest propagation losses. As for effective index, the families of κ_{eff} curves for the planar TE_{00} and fiber HE_{11} modes are qualitatively almost identical; values for the planar geometry being marginally lower because a slightly smaller fraction of the mode extends into the cladding (0.10% of the mode field for the planar waveguide as compared to 0.12% for the fiber, at a wavelength $\lambda = 275$ nm). The fiber TE_{01} mode provides the lowest values of κ_{eff} (with only 0.06% of mode field in the

Optical Materials EXPRESS

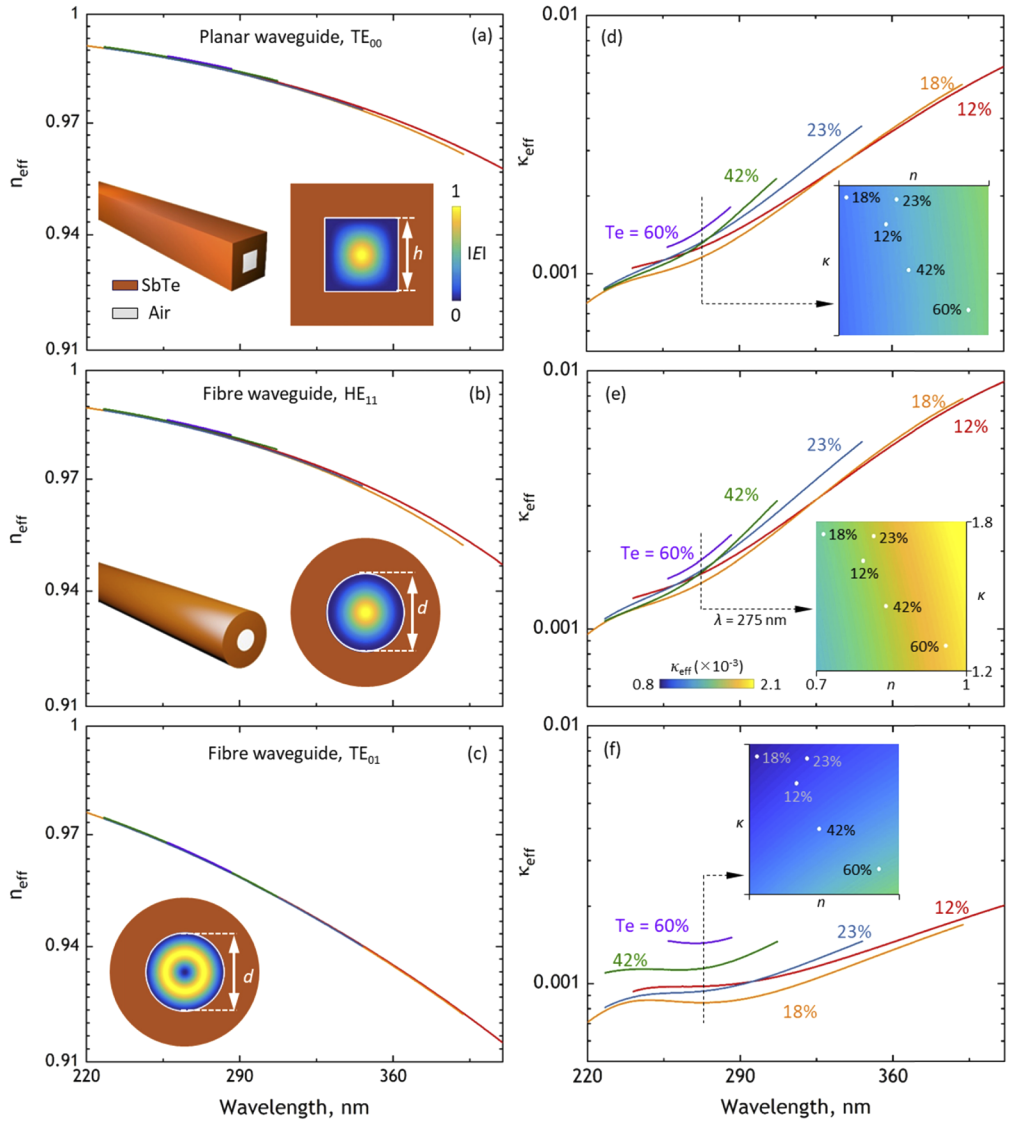

Fig. 2. Low-index hollow-core UV waveguides. Spectral dispersion of (a-c) effective index and (d-f) corresponding extinction coefficient for selected modes of square- and circular-section (nominally planar and fiber type) hollow-core waveguides with SbTe cladding of varying composition [as presented in Fig. 1]: (a, d) planar waveguide TE_{00} mode; (b, e) Fiber HE_{11} mode; (c, f) Fiber TE_{01} mode. A core size $h, d = 1200$ nm is assumed in all cases. Insets to (a-c) show cross-sections of the waveguides with overlaid maps of the electric field distribution in the core. Insets to (d-f) show effective extinction coefficient at $\lambda = 275$ nm as a function of the intrinsic refractive index and extinction coefficient of the cladding [n, κ ranges and κ_{eff} scale as per (e) in all cases] with points overlaid in this parameter space for the five SbTe compositions under consideration.

Optical Materials EXPRESS

cladding), as is expected for a hollow cylindrical metallic waveguide [29] - the compositions of SbTe considered here have negative values of ε_1, the real part of relative permittivity, over the spectral range where they satisfy the waveguiding condition that $n < n_{eff} < 1$.

Propagation distances L^* increase with increasing core size (diameter d or side length h), as shown in Fig. 3, reaching 120 μm (437λ) for an operating wavelength $\lambda = 275$ nm at a core size of 2 μm (~7λ). In accordance with the effective extinction coefficients plotted in Fig. 2 – the extent to which the evanescent tail of the guided mode lies within the cladding, for a given core size the planar (square-section) waveguide TE_{00} mode has a slightly longer propagation length than the fiber HE_{11} mode, while that of the fiber TE_{01} mode is the longest overall. The inset to Fig. 3 shows bend losses for the three modes. By virtue of its ideal cylindrical geometry about the propagation direction, losses for the fiber HE_{11} mode increase less rapidly with decreasing radius of curvature r than those of the planar waveguide TE_{00} mode, and for radii less than ~$10h$ (12 μm) the latter becomes the highest loss mode of the three considered here.

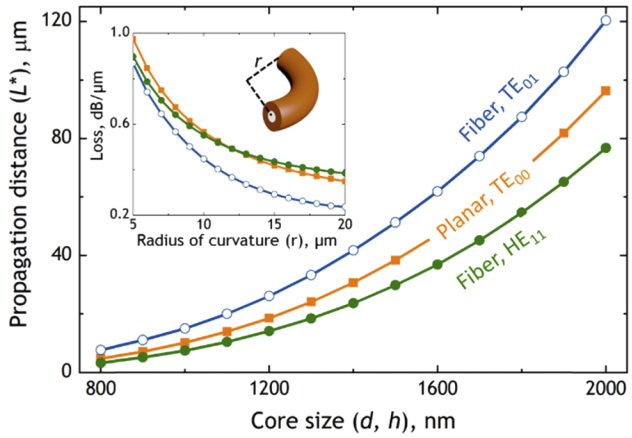

Fig. 3. Propagation constants in SbTe hollow-core UV waveguides. Propagation distance L^* as a function of core size for selected modes (as labelled) of planar (square-section) and fiber (circular-section) hollow-core $Sb_{4.1}Te_{0.9}$ waveguides at a wavelength of 275 nm. The inset shows propagation loss as a function of radius of curvature r for core sizes d, $h = 1.2$ μm.

As noted above, the intrinsic material losses of SbTe are high compared to those of media that would conventionally be employed in the fabrication of optical waveguides, and propagation distances (Fig. 3) are correspondingly relatively short. At near-infrared wavelengths, for example, hollow-core (photonic crystal) silica fibers and solid-core silicon-on-insulator strip waveguides provide propagation distances respectively of order 10 m ($10^7\lambda$) [30] and 70 mm ($10^4\lambda$) [31]; at near-UV wavelengths, solid-core beta-barium borate and antiresonant hollow-core silica waveguides can offer propagation lengths respectively of order ~4 mm ($10^4\lambda$) [3] and ~1m ($10^6\lambda$) [12], albeit at relatively large core sizes up to ~50λ (λ being the free-space wavelength in all cases). However, the potential benefit of hollow-core SbTe guides lies not in their use for point-to-point signal transmission over any distance (even at intra-chip level), but in their ability to provide small-core (few-λ), step-index hollow-core guiding functionality at short wavelengths and in the availability of alloy composition as an additional degree of freedom in waveguide design (e.g. setting of cut-off wavelength for light guiding through specification of cladding index n).

In sensing applications, the key advantage of hollow waveguides is that they confine the optical mode and analyte in the same volume, making propagation highly sensitive to changes in analyte refractive index and/or extinction coefficient. For example, in a basic interferometric configuration, one would be concerned with the phase retardation arising from the introduction of

Optical Materials EXPRESS

an analyte $\delta\phi = 2\pi\delta n_{eff}L/\lambda$, where Δn_{eff} is the change in effective index induced by the presence of the analyte and L is the interaction length. In a hollow core geometry, the former can be as large (approximately) as $n_{analyte}-1$ (where $n_{analyte}$ is the intrinsic index of the analyte). As such they can yield characteristic L_π lengths (over which a π phase shift accumulates, maximizing interferometric contrast) that are orders of magnitude shorter than are achievable with solid-core waveguides relying upon evanescent field interaction with a surrounding analyte, while also being far less sensitive (indeed, almost insensitive) to core size. In the present case, these distances can be in the few micron range, i.e. comfortably shorter than L^* propagation decay lengths (Fig. 3) and compatible with chip-scale device architectures. Equivalent considerations apply to required interaction lengths in absorptive sensors and other (e.g. spectroscopic, frequency conversion) applications.

3. Conclusion

In summary, we consider opportunities presented by the chalcogenide semiconductor antimony telluride as a stoichiometrically-controllable low-index medium for mid- to near-UV wavelengths. With sub-unitary ($n < 1$) refractive indices over a wavelength range extending from as low as 220 to as high as 400 nm, SbTe can facilitate step-index hollow-core waveguiding in the UV range. In offering propagation lengths of order 100 μm at few-wavelength core sizes, this material family presents intriguing possibilities for the realization of ultra-compact integrated UV photonic, optoelectronic and optofluidic devices. Propagation losses will constrain these to simple, short-reach architectures. However, SbTe may find advantage in compatibility with CMOS lithographic processes for micro- to nanoscale photonic and optoelectronic device fabrication, e.g. whereby integrated UV source, waveguide, and detector could be manufactured on a single substrate. The material platform also provides for the specification of waveguide properties via selection of alloy composition (i.e. cladding index and extinction coefficients) as well as the generic design parameters of core geometry and size - we present data here for a set of five specific Sb:Te ratios representative of the available continuously tunable compositional parameter space. In planar device configurations, a prescribed gradient of composition over the surface [32] may add functionality, e.g. in tuning the effective indices of an array of geometrically identical waveguides. SbTe cannot be conventionally drawn (like silica or other glasses) into the cylindrical form of a hollow-core optical fiber, but a range of other techniques exist for the manufacture of short-length specialty fibers. Such a structure might be realized, for example, by pressure-assisted melt-filling of or extrusion through a mould [33]; 'lithography-assisted' preform fabrication [34]; or coating the inner surface of a silica hollow-core fiber via chemical vapor or solution-based deposition techniques [35,36]. Planar hollow-core SbTe waveguides can be fabricated lithographically (e.g. by etching a trench of the required dimensions into a Si wafer, coating with SbTe, and bonding 'face-to-face' with a second SbTe-coated wafer [37]).

Funding

Engineering and Physical Sciences Research Council (EP/M009122/1); Ministry of Education - Singapore (MOE2016-T3-1-006); China Scholarship Council (201708440254).

Disclosures

The authors declare no conflicts of interest.

Data Availability: No new materials data are presented in this article.

Optical Materials EXPRESS

References

1. M. Soltani, R. Soref, T. Palacios, and D. Englund, "AlGaN/AlN integrated photonics platform for the ultraviolet and visible spectral range," Opt. Express **24**(22), 25415–25423 (2016).
2. O. S. Wolfbeis, "Fiber-Optic Chemical Sensors and Biosensors," Anal. Chem. **80**(12), 4269–4283 (2008).
3. G. Poberaj, R. Degl'Innocenti, C. Medrano, and P. Günter, "UV integrated optics devices based on beta-barium borate," Opt. Mater. **31**(7), 1049–1053 (2009).
4. G. N. West, W. Loh, D. Kharas, C. Sorace-Agaskar, K. K. Mehta, J. Sage, J. Chiaverini, and R. J. Ram, "Low-loss integrated photonics for the blue and ultraviolet regime," APL Photonics **4**(2), 026101 (2019).
5. T.-J. Lu, M. Fanto, H. Choi, P. Thomas, J. Steidle, S. Mouradian, W. Kong, D. Zhu, H. Moon, K. Berggren, J. Kim, M. Soltani, S. Preble, and D. Englund, "Aluminum nitride integrated photonics platform for the ultraviolet to visible spectrum," Opt. Express **26**(9), 11147–11160 (2018).
6. M. Stegmaier, J. Ebert, J. M. Meckbach, K. Ilin, M. Siegel, and W. H. P. Pernice, "Aluminum nitride nanophotonic circuits operating at ultraviolet wavelengths," Appl. Phys. Lett. **104**(9), 091108 (2014).
7. D. J. Blumenthal, "Photonic integration for UV to IR applications," APL Photonics **5**(2), 020903 (2020).
8. J. C. Knight, T. A. Birks, P. S. J. Russell, and D. M. Atkin, "All-silica single-mode optical fiber with photonic crystal cladding," Opt. Lett. **21**(19), 1547–1549 (1996).
9. M. K. Mridha, D. Novoa, S. T. Bauerschmidt, A. Abdolvand, and P. S. J. Russell, "Generation of a vacuum ultraviolet to visible Raman frequency comb in H2-filled kagomé photonic crystal fiber," Opt. Lett. **41**(12), 2811–2814 (2016).
10. M. Kumar, "A hollow waveguide Bragg reflector: A tunable platform for integrated photonics," Opt. Laser Technol. **65**, 5–13 (2015).
11. G. T. Jasion, J. R. Hayes, N. V. Wheeler, Y. Chen, T. D. Bradley, D. J. Richardson, and F. Poletti, "Fabrication of tubular anti-resonant hollow core fibers: modelling, draw dynamics and process optimization," Opt. Express **27**(15), 20567–20582 (2019).
12. A. Hartung, J. Kobelke, A. Schwuchow, K. Wondraczek, J. Bierlich, J. Popp, T. Frosch, and M. A. Schmidt, "Double antiresonant hollow core fiber – guidance in the deep ultraviolet by modified tunneling leaky modes," Opt. Express **22**(16), 19131–19140 (2014).
13. B. J. Eggleton, B. Luther-Davies, and K. Richardson, "Chalcogenide photonics," Nat. Photonics **5**(3), 141–148 (2011).
14. B. Gholipour, "The promise of phase-change materials," Science **366**(6462), 186–187 (2019).
15. M. Wuttig, H. Bhaskaran, and T. Taubner, "Phase-change materials for non-volatile photonic applications," Nat. Photonics **11**(8), 465–476 (2017).
16. A.-K. U. Michel, M. Wuttig, and T. Taubner, "Design Parameters for Phase-Change Materials for Nanostructure Resonance Tuning," Adv. Opt. Mater. **5**(18), 1700261 (2017).
17. D. Piccinotti, B. Gholipour, J. Yao, K. F. MacDonald, B. E. Hayden, and N. I. Zheludev, "Stoichiometric Engineering of Chalcogenide Semiconductor Alloys for Nanophotonic Applications," Adv. Mater. **31**(14), 1807083 (2019).
18. D. Piccinotti, B. Gholipour, J. Yao, K. F. Macdonald, B. E. Hayden, and N. I. Zheludev, "Compositionally controlled plasmonics in amorphous semiconductor metasurfaces," Opt. Express **26**(16), 20861–20867 (2018).
19. B. Gholipour, A. Karvounis, J. Yin, C. Soci, K. F. MacDonald, and N. I. Zheludev, "Phase-change-driven dielectric-plasmonic transitions in chalcogenide metasurfaces," NPG Asia Mater. **10**(6), 533–539 (2018).
20. B. Gholipour, D. Piccinotti, A. Karvounis, K. F. MacDonald, and N. I. Zheludev, "Reconfigurable Ultraviolet and High-Energy Visible Dielectric Metamaterials," Nano Lett. **19**(3), 1643–1648 (2019).
21. K. Shportko, S. Kremers, M. Woda, D. Lencer, J. Robertson, and M. Wuttig, "Resonant bonding in crystalline phase-change materials," Nat. Mater. **7**(8), 653–658 (2008).
22. J.-Y. Ou, J.-K. So, G. Adamo, A. Sulaev, L. Wang, and N. I. Zheludev, "Ultraviolet and visible range plasmonics in the topological insulator Bi1.5Sb0.5Te1.8Se1.2," Nat. Commun. **5**(1), 5139 (2014).
23. K. Kuroda, M. Ye, A. Kimura, S. V. Eremeev, E. E. Krasovskii, E. V. Chulkov, Y. Ueda, K. Miyamoto, T. Okuda, K. Shimada, H. Namatame, and M. Taniguchi, "Experimental Realization of a Three-Dimensional Topological Insulator Phase in Ternary Chalcogenide $TlBiSe_2$," Phys. Rev. Lett. **105**(14), 146801 (2010).
24. H. N. S. Krishnamoorthy, G. Adamo, J. Yin, V. Savinov, N. I. Zheludev, and C. Soci, "Infrared dielectric metamaterials from high refractive index chalcogenides," Nat. Commun. **11**(1), 1692 (2020).
25. W. Shi, L. Zhou, S. Song, J. Yang, and H. Zhang, "Hydrothermal Synthesis and Thermoelectric Transport Properties of Impurity-Free Antimony Telluride Hexagonal Nanoplates," Adv. Mater. **20**(10), 1892–1897 (2008).
26. M. H. R. Lankhorst, B. W. S. M. M. Ketelaars, and R. A. M. Wolters, "Low-cost and nanoscale non-volatile memory concept for future silicon chips," Nat. Mater. **4**(4), 347–352 (2005).
27. Y. Yirmiyahu, A. Niv, G. Biener, V. Kleiner, and E. Hasman, "Excitation of a single hollow waveguide mode using inhomogeneous anisotropic subwavelength structures," Opt. Express **15**(20), 13404–13414 (2007).
28. F. K. Fatemi, M. Bashkansky, E. Oh, and D. Park, "Efficient excitation of the TE01 hollow metal waveguide mode for atom guiding," Opt. Express **18**(1), 323–332 (2010).
29. E. A. J. Marcatili and R. A. Schmeltzer, "Hollow Metallic and Dielectric Waveguides for Long Distance Optical Transmission and Lasers," Bell Syst. Tech. J. **43**(4), 1783–1809 (1964).
30. N. V. Wheeler, A. M. Heidt, N. K. Baddela, E. N. Fokoua, J. R. Hayes, S. R. Sandoghchi, F. Poletti, M. N. Petrovich, and D. J. Richardson, "Low-loss and low-bend-sensitivity mid-infrared guidance in a hollow-core–photonic-bandgap fiber," Opt. Lett. **39**(2), 295–298 (2014).

Optical Materials EXPRESS

31. G. Z. Mashanovich, F. Y. Gardes, D. J. Thomson, Y. Hu, K. Li, M. Nedeljkovic, J. S. Penades, A. Z. Khokhar, C. J. Mitchell, S. Stankovic, R. Topley, S. A. Reynolds, Y. Wang, B. Troia, V. M. N. Passaro, C. G. Littlejohns, T. D. Bucio, P. R. Wilson, and G. T. Reed, "Silicon Photonic Waveguides and Devices for Near- and Mid-IR Applications," IEEE J. Sel. Top. Quantum Electron. **21**(4), 407–418 (2015).
32. S. Guerin and B. E. Hayden, "Physical Vapor Deposition Method for the High-Throughput Synthesis of Solid-State Material Libraries," J. Comb. Chem. **8**(1), 66–73 (2006).
33. N. Granzow, S. P. Stark, M. A. Schmidt, A. S. Tverjanovich, L. Wondraczek, and P. S.-J. Russell, "Supercontinuum generation in chalcogenide silica step-index fibers," Opt. Express **19**(21), 21003–21010 (2011).
34. B. Gholipour, P. Bastock, L. Cui, C. Craig, K. Khan, D. W. Hewak, and C. Soci, "Lithography Assisted Fiber-Drawing Nanomanufacturing," Sci. Rep. **6**(1), 35409 (2016).
35. P. J. A. Sazio, A. Amezcua-Correa, C. E. Finlayson, J. R. Hayes, T. J. Scheidemantel, N. F. Baril, B. R. Jackson, D.-J. Won, F. Zhang, E. R. Margine, V. Gopalan, V. H. Crespi, and J. V. Badding, "Microstructured Optical Fibers as High-Pressure Microfluidic Reactors," Science **311**(5767), 1583–1586 (2006).
36. A. H. Lewis, F. De Lucia, W. Belardi, C.-C. Huang, J. R. Hayes, F. Poletti, D. Hewak, and P. J. A. Sazio, "Composite material anti-resonant optical fiber electromodulator with a 35 dB depth," Opt. Lett. **45**(5), 1132–1135 (2020).
37. J. F. Bauters, M. J. R. Heck, D. D. John, J. S. Barton, C. M. Bruinink, A. Leinse, R. G. Heideman, D. J. Blumenthal, and J. E. Bowers, "Planar waveguides with less than 0.1 dB/m propagation loss fabricated with wafer bonding," Opt. Express **19**(24), 24090–24101 (2011).